Molecular Dynamics Studies of Caspase-3

M. Sulpizi,* U. Rothlisberger,* and P. Carloni[†‡]

*Laboratory of Computational Chemistry and Biochemistry, Federal Institute of Technology (EPFL) CH-1015 Lausanne, Switzerland; [†]SISSA, International School for Advanced Studies, via Beirut 2-4, 34013 Trieste, Italy; and [‡]INFM DEMOCRITOS Center for Numerical Simulation, Italy

ABSTRACT Caspase-3 is a fundamental target for pharmaceutical interventions against a variety of diseases involving disregulated apoptosis. The enzyme is active as a dimer with two symmetry-related active sites, each featuring a Cys-His catalytic dyad and a selectivity loop, which recognizes the characteristic DEVD pattern of the substrate. Here, a molecular dynamics study of the enzyme in complex with two pentapeptide substrates DEVDG is presented, which provides a characterization of the dynamic properties of the active form in aqueous solution. The mobility of the substrate and that of the catalytic residues are rather low indicating a distinct preorganization effect of the Michaelis complex. An essential mode analysis permits us to identify coupled motions between the two monomers. In particular, it is found that the motions of the two active site loops are correlated and tend to steer the substrate toward the reactive center, suggesting that dimerization has a distinct effect on the dynamic properties of the active site regions. The selectivity loop of one monomer turns out to be correlated with the N-terminal region of the p12 subunit of the other monomer, an interaction that is also found to play a fundamental role in the electrostatic stabilization of the quaternary structure. To further characterize the specific influence of dimerization on the enzyme essential motions, a molecular dynamics analysis is also performed on the isolated monomer.

INTRODUCTION

Caspases are a family of cysteine proteases involved in all apoptosis pathways (Salvesen and Dixit, 1997). Their disregulation is involved as a key factor for the development of a variety of diseases, including Alzheimer's (Shimohama, 2000), Parkinson's (Jordan et al., 2000), and cancer (Kaufmann and Gores, 2000)).

Fourteen different caspases have been characterized so far (Talanian et al., 2000). Although the activity and specificity patterns of these enzymes are clearly distinct (Ventimiglia et al., 2001), their overall reaction mechanism is expected to be similar (Wilson et al., 1994). All of these enzymes recognize specific four-residue sequences and cleave peptide bonds located strictly after an Asp group. In addition, the three-dimensional (3D) structures of caspases determined so far (caspase-1 (Rano et al., 1997; Okamoto et al., 1999; Wei et al., 2000; Huang et al., 2001); caspase-3 (Rotonda et al., 1996; Mittl et al., 1997; Lee et al., 2000; Riedl et al., 2001); caspase-7 (Wei et al., 2000; Huang et al., 2001); and caspase-8 (Watt et al., 1999; Blanchard et al., 1999; Xu et al., 2001)) are highly homologous and structurally alike (Walker et al., 1994). They all form homodimers of heterodimers, in which each monomer consists of a small and a large subunit that form a central core of six β-sheets surrounded by five α-helices (Fig. 1). Finally, the conformational properties of the two catalytically relevant residues (a Cys and a His residue (Fersht, 1997)) are highly similar.

Submitted April 18, 2002, and accepted for publication November 25, 2002.

Address reprint requests to U. Rothlisberger, Laboratory of Computational Chemistry and Biochemistry, Federal Institute of Technology (EPFL) CH-1015 Lausanne, Switzerland. Tel.: +41-21-693 0321; Fax: +41-21-693 0320; E-mail: ursula.roethlisberger@epfl.ch.

0006-3495/03/04/2207/09 $2.00

In living cells, caspases exist in the form of inactive precursors or procaspases that can be activated on demand via different pathways. Recent experiments have shown that for certain caspases, activity can be induced via dimerization (Muzio et al., 1998; Yang et al., 1998; Colussi et al., 1998; Renatus et al., 2001). So far, the mechanistic aspects of caspase activity have solely been inferred from indirect evidence drawn from structural information on enzyme/inhibitor complexes. However, to gain a more comprehensive picture of the enzymatic reaction mechanism, it is of importance to characterize the structural and conformational properties of the substrate-enzyme complex and to analyze its dynamical features.

In this paper, we present one of the first attempts to use molecular simulations to gain insights on structure/function relationships in an exemplary member of the caspase family, the downstream caspase-3. Caspase-3 acts as one of the central death executioners and as such is involved in virtually every model of apoptosis (Porter and Janicke, 1999). It is also implicated in a large number of human diseases for which either excessive (such as in the case of ischemic damage and neurodegenerative disorders) or insufficient (e.g., for cancer and autoimmune diseases) apoptosis occurs (Talanian et al., 2000). The enzyme exhibits a large substrate diversity, as it cleaves a variety of proteins involved in cell maintenance and/or repair, among them poly(ADP-ribose) polymerase, p21-activated kinase 2, gelsolin, and DNA-dependent protein kinase (Cohen, 1997; Liu et al., 1997; Enari et al., 1998). It is one of the biochemically (Stennicke and Salvesen, 1997) and structurally best-characterized isoenzymes.

In this work, we have used molecular dynamics (MD) simulations and electrostatic calculations to investigate dynamics and energetics of the enzyme in complex with its

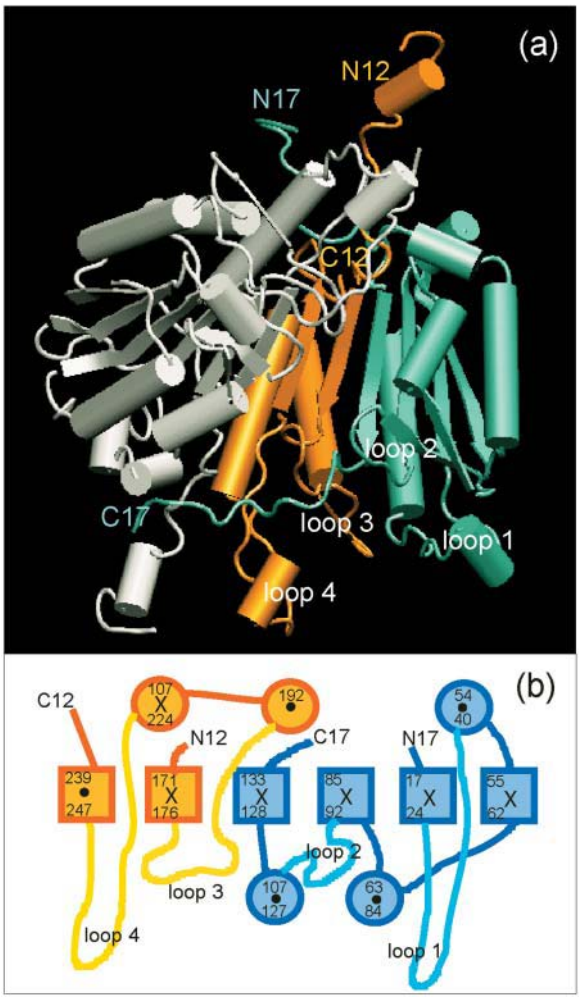

FIGURE 1 (*a*) Overall structure of caspase-3 dimer. Only one of the two monomer units is shown in color. The large subunit (p17) is reported in blue, the small subunit (p12) in orange. The subunit termini and the active site loops are labeled. (*b*) Schematic picture of the topology of the caspase-3 monomer. Helices (*circles*); β-sheets (*squares*). Elements pointing out of the sheet are indicated with a dot, whereas a cross indicates elements oriented in the opposite direction. Numbering of protein residues is indicated according to Rotonda et al. (1996). The active site region is formed by four loops (loops 1–4). The color scheme is the same as for *a*.

DEVDG substrate. The simulations, which are based on the x-ray structure of the human isoenzyme complexed with the aldehyde tetrapeptide Ac-DEVD-CHO (Ac = acetyl group) (Rotonda et al., 1996), are performed for the dimeric form, which is present at physiological concentrations (Talanian et al., 1996). The investigation of the dimer properties are complemented by reference calculations on the isolated monomer, which are meant to provide information on the relevance of dimerization for caspase-3 stability and function.

Our calculations suggest that the large-scale main global motions on the nanosecond timescale involve a correlated motion of the two active sites. Furthermore, they help elucidate active site differences between caspases and other cysteine proteases of the papain family, such as papain itself (Drenth et al., 1968; Kamphuis et al., 1984), cathepsins B (Musil et al., 1991; Jia et al., 1995; Turk et al., 1995; Yamamoto et al., 2000), L (Coulombe et al., 1996; Guncar et al., 1999), K (Zhao et al., 1997; Yamashita et al., 1997; Thompson et al., 1997), H (Guncar et al., 1998), and S (Fengler and Brandt, 1998); *Trypanosoma cruzi* enzyme cruzain (Gillmor et al., 1997; Brinen et al., 2000); and bleomycin hydrolase and deubiquitinating enzyme (Johnston et al., 1997; Johnston et al., 1999). As pointed out previously (Sulpizi et al., 2003), the catalytically active His residue (His-237) adopts a different conformation than that found in other cysteine proteases. Specifically, the torsional parameters χ_1 and χ_2 of His-237 (Rano et al., 1997; Okamoto et al., 1999; Wei et al., 2000; Huang et al., 2001; Rotonda et al., 1996; Mittl et al., 1997; Lee et al., 2000; Riedl et al., 2001; Wei et al., 2000; Huang et al., 2001; Watt et al., 1999; Blanchard et al., 1999; Xu et al., 2001)) lie in a different region of the Ramachandran plot than those of the catalytic histidine in other crystallized cysteine proteases such as papain (Drenth et al., 1968; Kamphuis et al., 1984) and cathepsin B (Musil et al., 1991; Jia et al., 1995; Turk et al., 1995; Yamamoto et al., 2000), L (Coulombe et al., 1996; Guncar et al., 1999), K (Zhao et al., 1997; Yamashita et al., 1997; Thompson et al., 1997), H (Guncar et al., 1998), and S (Fengler and Brandt, 1998) (Fig. 2 *a*). It is therefore of interest to monitor the dynamical evolution of the χ_1 and χ_2 angles during the MD simulation.

METHODS

Structural model

Our models are based on the structure of caspase-3 covalently bound to the tetrapeptide aldehyde Ac-DEVD-COH inhibitor (Rotonda et al., 1996) (PDB (Sussman et al., 1998) ENTRY: 1PAU). These inhibitors contain the preferred recognition motif of caspase-3 (DEVD) (Rotonda et al., 1996), and its Asp-4′ carbonylic carbon forms a bond with the sulfur atom of the catalytically active cysteine (Cys-285). In our model, the C-S bond is removed. Furthermore, an additional Gly residue is added according to the poly-ADP ribose polymerase (PARP) sequence, to generate the minimal, yet fully functional, substrate of the enzyme (Lazebnik et al., 1994).

Both the monomeric and homodimeric forms are considered. Hydrogen atoms, invisible to the x-ray diffraction experiment, are added assuming standard bond lengths and angles. In the active sites, the catalytic residues Cys-285 and His-237 are assumed to be in the neutral state. This is consistent with the presently accepted mechanism, which postulates that the catalytic Cys is deprotonated during its nucleophilic attack of the substrate (Nicholson et al., 1995). Consistently, test MD calculations on the dimeric form in which Cys-285 and His-237 are assumed negatively and positively charged, respectively, show that the system is unstable. In particular, the active site undergoes large structural rearrangements within already the first 0.5 ns indicated by an increasing distance of the substrate from the active site.

The dimer and the monomer are immersed in a box of edges $86.6 \times 73.3 \times 76.4$ Å^3 and $85.0 \times 72.0 \times 60.0$ Å^3, containing 12,858 and 11,091 water molecules, respectively. (The density of the solvent in our system is 1g/cm^3.) Their overall negative charge is neutralized by adding six sodium ions, respectively, located close to residues Glu-191, Glu-213, Asp-313 in each

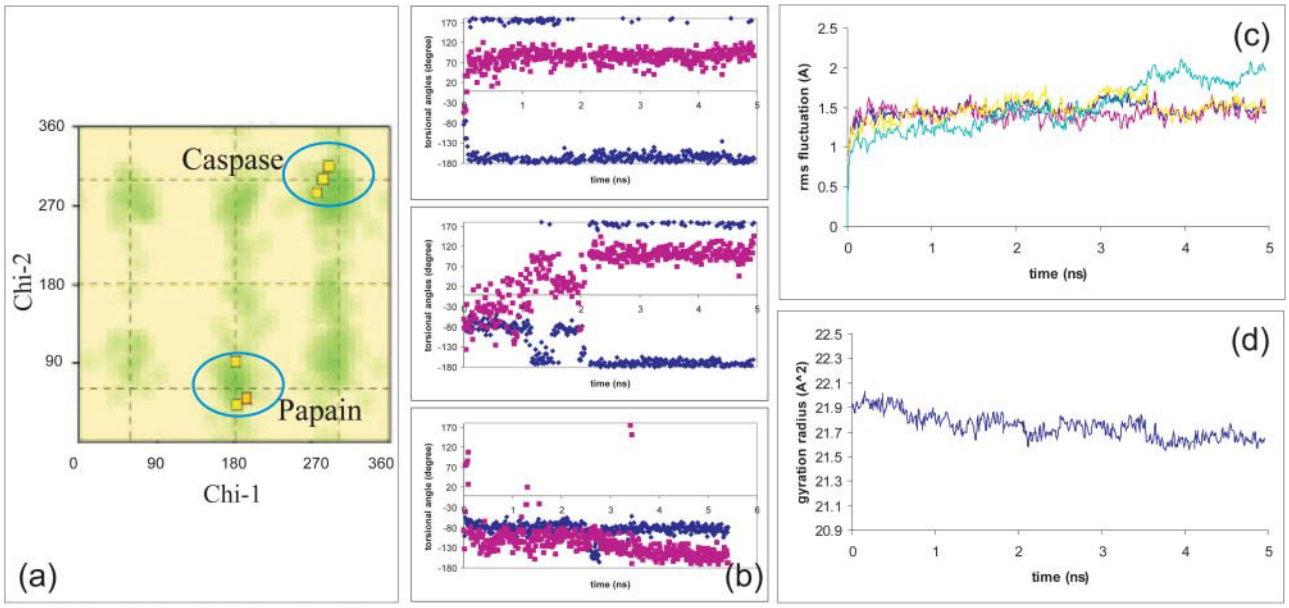

FIGURE 2 Torsional parameters for the catalytic histidine. (*a*) Ramachandran plot for the torsional angles of catalytic histidines in some cysteine proteases. Regions for χ_1 and χ_2 indicated with a blue circle correspond to papain-like and caspase-like crystallographic configurations. (*b*) Time evolution for χ_1 and χ_2 for monomer A (*top*), monomer B (*middle*) and isolated monomer (*bottom*), respectively. (*c*) Time dependence of the RMS deviation (Å/atom) from the minimized x-ray structure of caspase-3 dimer (*blue line*), monomer A (*magenta*), monomer B (*yellow*), and isolated monomer (*cyan*). (*d*) Radius of gyration of the caspase-3 dimer.

subunit. As these residues are located far from the active site, their electrostatic field effect on the reactants is expected to be very small.

MD simulations

Classical MD simulations are performed for both monomer and dimer with the program packages GROMOS96 (van Gunsteren et al., 1996) augmented with a P3M treatment of the long-range electrostatic interactions (Hunenberger, 2000), and GROMACS (Lindahl et al., 2001). The mesh used for the P3M calculation is 64 × 64 × 64. A leap-frog integration algorithm with a time step of 1.5 fs is used throughout with all bond lengths kept fixed applying a SHAKE algorithm (Ryckaert et al., 1977). Constant temperature-constant volume simulations are performed by coupling the system to a Berendsen thermostat (Berendsen et al., 1984) with a relaxation time of 0.1 ps. After 0.1 ns of solvent equilibration, keeping the coordinates of the heavy atoms fixed, the whole system is gently heated to 300 K and equilibrated for 0.5 ns. Finally, data is collected during 4.5 ns for subsequent analysis.

Calculated properties

Root mean square (RMS) fluctuations of the C_α atoms and the radius of gyration of the protein are used as stability measures of the protein structure. An essential dynamics analysis of the protein motions was performed following the procedures of Amadei et al. (1993), de Groot et al. (1996), and Garcia and Hummer (1999). The large-scale movements (i.e., those in the essential subspace) are represented by the eigenvectors of the correlation matrix $\langle(x-\langle x\rangle)(x-\langle x\rangle)^T\rangle$, where x represents the position vectors of the C_α atoms. It is possible to limit the analysis to the first few eigenvectors because they take into account the major part of the protein motion (the first 10 eigenvalues correspond to ~50% of the global motion as already reported for numerous other cases (Amadei et al., 1993). Each structure along the trajectory is fitted to the starting configuration, eliminating global translational and rotational degrees of freedom. The fitting is performed using only the C_α atoms belonging to the secondary structure elements of the protein, namely the β-sheet core and the α-helical bundle, which surrounds it (Fig. 1). The highly flexible regions belonging to the chain termini and the loops embracing the substrates are not taken into account.

Calculations of the electric field of the protein/water system on substrate Asp-4′ and water exposed Asp-183 carboxyl carbons as a function of simulated time are performed using a simple Coulomb formula with a dielectric constant of 1 and GROMOS96 atomic point charges (van Gunsteren et al., 1996).

The electrostatic free energy of binding ΔE at the monomer-monomer interface for the dimer is estimated by solving the Poisson-Boltzmann equation(Leach, 1996) for the crystal structure (Rotonda et al., 1996). ΔE is defined as $E_{\text{dimer}} - E_{\text{monomer A}} - E_{\text{monomer B}}$, where E_{dimer} is the electrostatic free energy of the dimer and $E_{\text{monomer A}}$ and $E_{\text{monomer B}}$ are the single monomer electrostatic free energies. Calculations were carried out on a grid of 201 points, with a temperature of 298 K and an ionic strength of 0.15 mM, using the program DELPHI (Gilson and Honig, 1988). The dielectric constants of the protein and water were set to 2 and 80, respectively. The focusing technique by Gilson and Honig (1988) was applied.

RESULTS

Overall stability

The RMS fluctuations of the C_α atoms of the dimeric form are small and converge to an average value of 1.5 Å after 0.5 ns, suggesting that the system is relatively stable over the explored timescale of 5 ns (Fig. 2 *c*, *blue line*). Interestingly, monomer A exhibits a slightly larger displacement in the first part (Fig. 2 *c*, *magenta line*), and monomer B in the second part of the simulation (Fig. 2 *c*, *yellow line*) suggesting some compensatory effects among the displacements of the two monomer units. However, this asymmetry does not persist

in the subsequent 1.5 ns. The gyration radius of the protein remains essentially constant, with a minimal shrinkage of 1.5% with respect to the x-ray data of the inhibitor complex (Fig. 2 *d*).

The isolated monomer, on the other hand, exhibits a higher value for the RMS fluctuations (around 2.0 Å) with an increasing trend (Fig. 2 *c*, *cyan line*), which originates mostly from a higher flexibility of the N- and C-termini (rmsd over the last 3 ns: 3.8 Å). These domains are located at the monomer-monomer interface in the dimer. In contrast, the main secondary structure elements are well preserved (rmsd over the last 3 ns: 1.0 Å). Major differences between the single unit in the monomer and dimer caspase-3 involve the regions of the termini and Loop 1 (Fig. 3, *left*).

Active sites: conformational properties

The active site comprises four loops (loops 1–4 in Fig. 1) and the model substrate. As pointed out in the introduction, the conformational properties of His-237 are different from those of other cysteine proteases. In our dynamics of the dimer, the χ_1 and χ_2 torsion angles of His-237 fluctuate largely (Fig. 2 *b*), sampling two regions, one in which the conformation of this residue resembles that of the crystal structure and the other in which χ_1 is increased by 120° and χ_2 by 240°, respectively, which resembles the one of other cysteine proteases.

The average distance between the catalytically essential Cys-285 and His-237 residues in both monomers ($\langle d_{SN} \rangle$) remains almost constant over the simulation time and exhibits only small fluctuations of 6%. Due to the presence of the substrate located in between these two residues, $\langle d_{SN} \rangle$ is slightly higher (6.8 Å) than the corresponding crystallographic value in the inhibitor complex (5.6 Å) (Table 1). The reactants are tightly fixed to the active site pocket as indicated by the short average distance between the sulfur atom of Cys-285 and the carbonylic carbon of Asp-4′ of the substrate $\langle d_{SC} \rangle$ (Table 1). Essentially $\langle d_{SC} \rangle$ is identical in both monomers and during 5% of the total time samples values of less than 3.1 Å. The occurrence of such short distances suggests that bond distance fluctuations promoting the reaction of the catalytic cysteine with the substrate can take place rather easily. In addition, the occurrence of such critical events is also favored by the rather strict preservation of the orientation of Cys-285 with respect to the Asp-4 carbonyl group ($\langle \varphi_{SCO} \rangle = 110° \pm 10$ in both monomers) (Table 1). This suggests a distinct preorganization effect of the Michaelis complex.

In the monomer, another region of the χ_1, χ_2 conformational space is populated (Fig. 2 *b*) with respect to that of the dimer, possibly connected to the different mobility of the active site loops (Fig. 2 *b*). However, as the conformational transitions occur very rarely (one or two times during the 5-ns simulation), this difference might be merely an artifact of the limited simulation time.

Correlated motions

An analysis of the essential dynamics of the protein (Amadei et al., 1993) enables a classification of the large-scale movements of the enzyme and allows investigating possible correlations of the two monomer units.

In the dimer, the lowest eigenvector of the correlation matrix corresponds to a global bending of the structure, which mainly involves the flexible regions (Fig. 4 *a*). The second largest eigenvector essentially corresponds to motions of the active site loops. In both monomers, the larger displacements are consistently found for loops 1 and 4

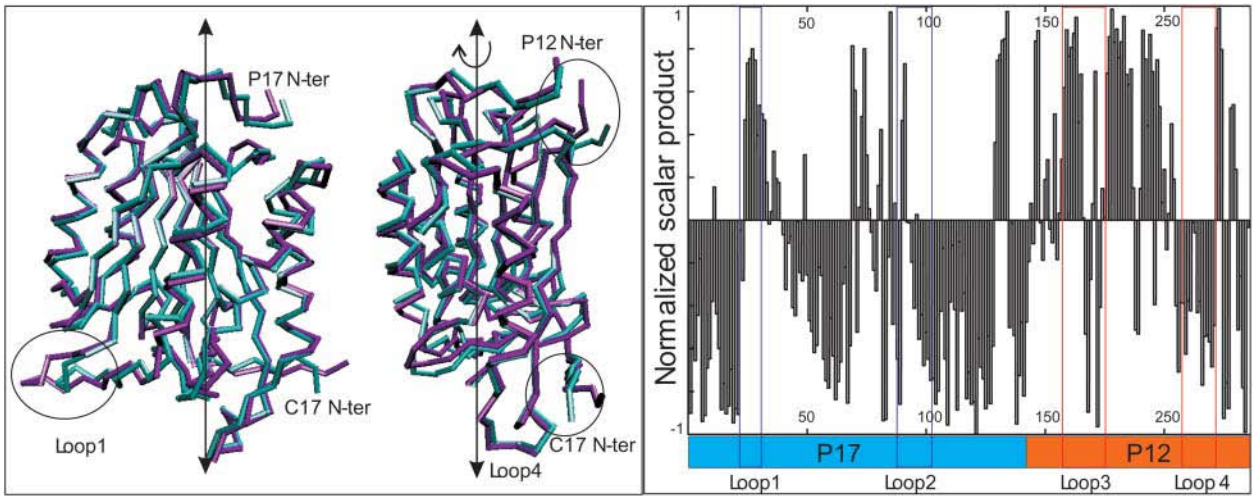

FIGURE 3 (*Left*) Average structure for a single monomer unit of caspase-3 in the simulation of the isolated monomer (*cyan*) and in the dimer (*magenta*). A side view is presented before and after a 90° rotation. (*Right*) Normalized scalar product of the eigenvector two of the caspase-3 monomer units in dimer and isolated monomer, as function of the residue number.

TABLE 1 Average values for some quantities characterizing the active sites of the two caspase-3 subunits

Monomer A	Cys-285 S – His-237 N	6.8 ± 0.3 (Å)
	Cys-285 S – Asp-4′ C	3.4 ± 0.2 (Å)
	Cys-285 S – Asp-4′ C – Asp-4′ O	110 ± 10 (degrees)
Monomer B	Cys-285 S – His-237 N	6.7 ± 0.3 (Å)
	Cys-285 S – Asp-4′ C	3.3 ± 0.2 (Å)
	Cys-285 S – Asp-4′ C – Asp-4′ O	110 ± 10 (degrees)
Crystal structure	Cys-285 S – His-237 N	5.6 (Å)

Average values and standard deviations are reported.

(according to the numbering in Fig. 1) (see Fig. 4 *b*). These loops embrace the substrate providing binding and selectivity. The substrate appears to be strongly tethered to the active site pocket, with the loops slightly closing in on the active site. This effect can be quantified by calculating the mean distance of the C_α atoms of the substrate from those C_α atoms of the active site region, which are in direct H-bonding contact with the substrate itself (Fig. 5 *a*). The average distance is almost constant, slightly lower than the one observed in the x-ray structure of the inhibitor complex, indicating that the loops tend to embrace the substrate in a somewhat tighter manner.

A projection of the total displacement along the second eigenvector, averaged over time, indicates that both monomers make essentially equal contributions to the motion along this mode, indicating that a correlation exists among the dynamics of the two active site regions. This conclusion is also supported by the result that a similar eigenvector (containing both active sites loop motion) is also obtained by diagonalization of the off-diagonal part of the covariance matrix corresponding to intermonomer correlations, confirming that the motion of the active site in the two monomers is not independent.

The third largest eigenvector corresponds to a global motion of the protein, describable as a sort of butterfly movement of the two monomers with the monomer interface as a hinge. A qualitative picture of the movement is shown in Fig. 4 *c*. The motion is completely symmetric in the two monomers indicating a mechanical coupling of the two units via the dimer interface. The fourth eigenvector correspond to an additional intermonomer movement, in form of a relative rotation (in opposite direction for the two monomers) around the axis of the β-sheet core (Fig. 4 *d*). In analogy to the other motions, also this twisting mode is equally present for both monomers.

Information about correlated motions is also obtained by an inspection of the covariance matrix of the displacements of the C_α atoms (Fig. 6 *a*). The covariance matrix contains contributions coming from both intermonomer and intramonomer correlated motions. In particular, it can be divided into four blocks corresponding respectively to internal motions of subunit A (A,A), internal motions of subunit B

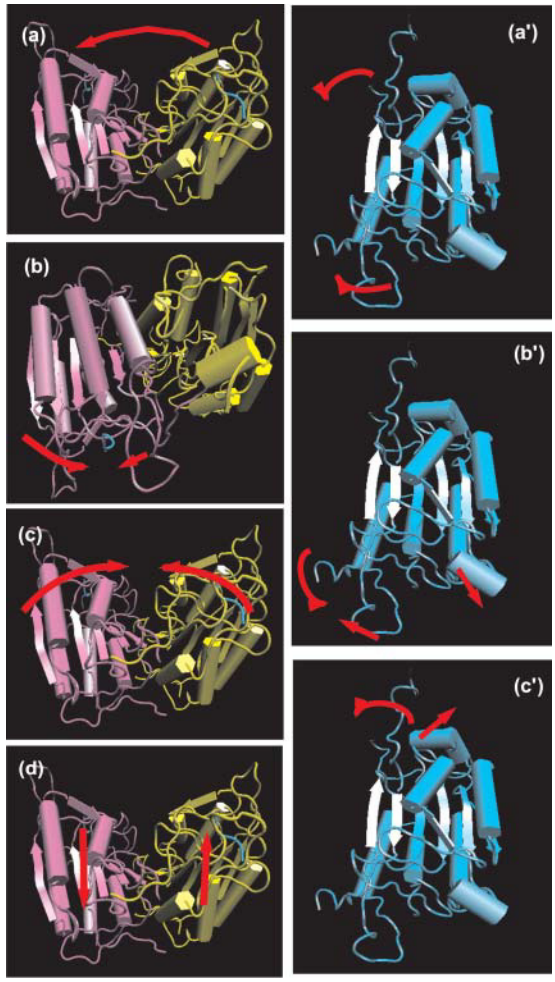

FIGURE 4 Schematic visualization of caspase-3 essential motions. *a*, *b*, *c*, and *d* motions correspond to the first, the second, the third, and the fourth eigenvector of the dimer dynamics. In *b* the motion is qualitatively indicated for one of the two active sites, monomer A, but is symmetric in the two monomers. *a*′, *b*′, and *c*′ essential motions correspond to eigenvectors one, two, and three for the isolated monomer.

(B,B), and coupled motion between subunit A and B ((A,B) and (B,A)) (see Fig. 6 *a*). Coupling among the two subunits can be quantified as the weight of the two symmetric (A,B) and (B,A) blocks over the global matrix. In particular, it turns out that the (A,B) and (B,A) blocks each account for 20% of the global covariance matrix. The global weight of matrices (A,B) and (B,A) has been calculated as $Tr(A,B)/(Tr(A,A) + Tr(B,B) + 2Tr(A,B))$.

Consistent with the essential mode analysis, the matrix features significant correlations between the two monomer units. In particular, these correlations involve loops 1, 2 (*blue circles* in Fig. 6 *a*), as well as 4 (selectivity loop) with the N-termini of both subunits (*red circles* in Fig. 6 *a*). In the dimer, the p17 C-terminus is in contact with the p12 N-terminus of the other monomer and contributes to the correlated motion observed in the covariance matrix.

In the monomer, the first eigenvalue involves a rearrange-

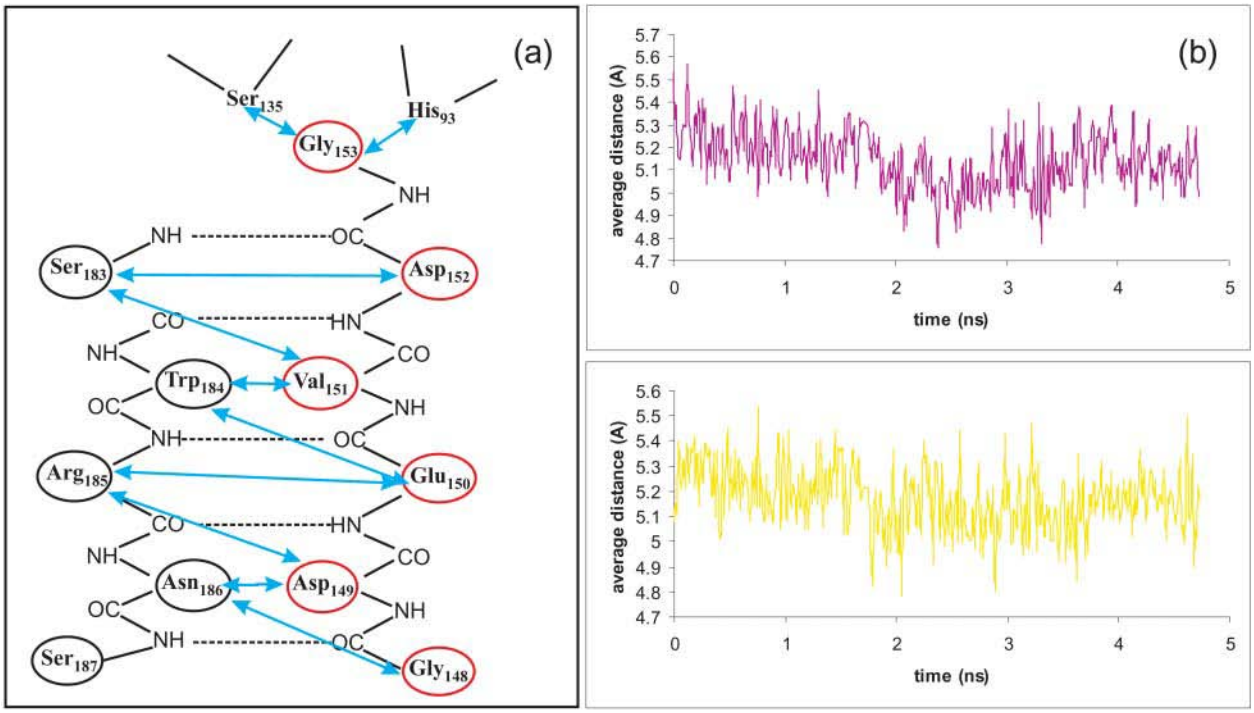

FIGURE 5 (*a*) Sketch of the binding of the substrate DEVDG in the active site pocket. The substrate backbone forms an antiparallel β-sheet with the substrate active site pocket. The distances calculated to estimate substrate flexibility in the active site pocket are shown as blue arrows. (*b*) Time evolution of the average substrate-pocket distances for monomer A (*magenta*) and for monomer B (*yellow*). The trend is also shown for both monomer units indicating that the substrate is slightly pushed closer to the enzyme pocket.

ment of the N-terminus of the p12 subunit (See Fig. 4 *a′*), which tends to bend toward the region of the monomer-monomer interface. This motion also involves the nearby loop connecting the last helix and the last β-sheet of the p17 subunit.

The second essential motion involves a rearrangement of the p17 C-terminus and the nearby loop 4 (see Fig. 4 *b′*) as well as contributions from loop 1. The third motion involves the region opposite to the enzyme active site: it is mainly involving the p12 C-terminus and a nearby loop (Fig. 4 *c′*).

The comparison between the essential eigenvectors of the monomer unit in the isolated monomer and in the dimer, reveals that the large amplitude motion of the active site loops is different in the monomer and dimer form. Indeed, in the second largest eigenvector, which involves motion of the active side loops in both cases, the scalar product of the eigenvector components (Fig. 3, *right*) provide positive correlation ($\sim$0.5) for loop 1 and negative correlation ($-$0.5) for loop 4 indicating that whereas the displacements involve similar protein regions, they have opposite directions.

Monomer-monomer interactions in the dimer

The monomer-monomer interface features mostly contacts between hydrophobic residues. However, an electrostatic analysis based on the Poisson-Boltzmann equation shows that some regions also provide an electrostatic stabilization to the binding free energy. The most stabilizing contributions arise from the interactions between Gln-385A and Pro-322B, Gln-385B and Pro-322A, as well as from Arg-266, Lys-278, and the three hydrophobic residues Val-323, Met-367, and Ala-382 (Fig. 6 *b*). Some destabilizing contributions arise from Asp-291, Glu-365, Arg-372, and Lys-383 (in both subunits A and B), which pay more in electrostatic dehydration penalty. It is interesting to note that the highly stabilizing Pro-322–Gln-385 contact is in the same region of dimer interface that shows a correlated motion in the correlation matrix.

DISCUSSION AND CONCLUSIONS

We have performed a 5-ns MD simulation of caspase-3 dimer in complex with the pentapeptide DEVDG model substrate. The structure is highly stable over the investigated timescale. The active site appears to be structurally similar to the one of the initial structural model (the x-ray structure of the Ac-DEVD-CHO inhibitor complex), although a certain flexibility is observed for the conformation of the catalytic His-237 (Fig. 2 *b*). Indeed, the χ_1 and χ_2 torsional angles, which describe the conformational properties of this residue, experience two different values during the dynamics (Fig. 2 *b*). One is similar to that of the initial model (Rotonda et al., 1996), and to those observed in all the x-ray structures of caspases (Rano et al., 1997; Okamoto et al., 1999; Wei et al.,

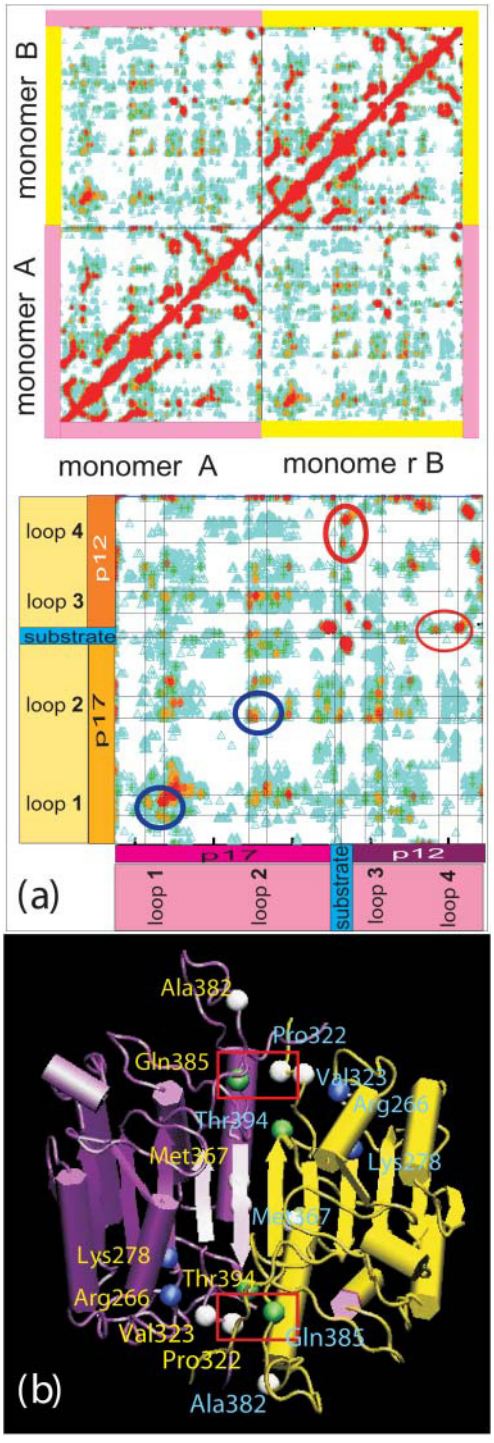

FIGURE 6 (*a*) Covariance matrix for the whole enzyme. Here, we report a symmetrized matrix over the two subunits. (*Top*) In the covariance matrix for each monomer it is possible to detect the elements defining the protein topology. (*Bottom*) Covariance matrix between monomer A and B. It is possible to see correlations between the loops 1 and 2 in the two monomers (*blue circles*) and a correlations between loop 4 (selectivity). (*b*) Major contributions to the monomer-monomer stabilizing energy. The eight residues with major contributions are reported with a ball. A red square identifies the recognition loop/N-terminus contact between Gln-385 and Pro-322 (two symmetric interactions for both monomer units are present). Residue hydrophobicity is also reported with a standard color code.

2000; Huang et al., 2001; Mittl et al., 1997; Lee et al., 2000; Riedl et al., 2001; Watt et al., 1999; Blanchard et al., 1999; Xu et al., 2001), whereas the other resembles that observed in all x-ray structures of the other cysteine proteases (Fig. 2 *a*).

Despite the high mobility of the His residues, the orientation of the substrates with respect to the residues forming the catalytic pocket is well maintained during the dynamics. The reduced flexibility of the active side residues and the substrate itself contrasts that of other proteases such as HIV-I protease (Piana et al., 2002) and dihydrofolate reductase (Radkiewicz and Brooks, 2000).

Novel information is obtained on the large-scale dynamics of caspase-3 dimer. We find that the motion of the two monomer units (and in particular of the two active site loops) is highly correlated (Fig. 6 *a*). This feature, which has already been observed in the dimeric enzyme Cu, Zn superoxide dismutase (Chillemi et al., 1997), is also consistent with the experimental findings that the dimeric form might be required for full activity. The loop displacements tend to push the substrate toward the active center (Fig. 5 *b*) possibly favoring more reactive configurations. The motion of loop 4 (the selectivity loop) is also correlated with that of the N-terminus of the p12 subunit of the other monomer (Fig. 6 *a*). Interestingly, this interaction also turns out to be relevant for the stabilization of the dimer interface (Fig. 6 *b*). Thus, our calculations fully support the claim, based on structural information, that this contact is essential for caspase activity (Riedl et al., 2001). Indeed, structural analysis of caspase-7 (which is highly homologous to caspase-3) and its proform suggested that this last interaction, which is present in the mature form and absent in procaspase-7 (Riedl et al., 2001) could be strictly related to activation.

For the sake of comparison, a molecular dynamics simulation over the same time scale has also been performed for the isolated monomer caspase-3. The monomeric form has never been observed with x-rays or NMR experiments, but could possibly exist in a small percentage of a monomer-dimer equilibrium under proper conditions (Talanian et al., 1996). In the case of the monomer dynamics, we find that the explored time scale is not sufficient to establish monomer instability or stability conclusively. However, the rms fluctuations exhibit a higher value with respect to the dimer and show an increasing trend indicating that a steady state has not yet been reached. Furthermore, the large-scale motions are different from the one of the dimer. In particular, the main motions of the monomer involve the termini, and in particular the p12 N- and p17 C-termini from opposite subunits, which form a cross contact that is of possible importance for the stability of the quaternary structure of dimeric caspase-3. Large amplitude motions of the active site loops 1 and 4 are also present in the isolated monomer, but they appear to be correlated to the p17 C-terminus motion and different from the active site loop motion in the dimer.

Thus, dimerization appears to have a direct effect on the

motions of the single subunits and in particular on the active site loops embracing the substrate. When the single monomer is considered in the isolated form, the motion of the active site loops is strongly influenced by the partial conformational rearrangement occurring at the termini level and involving a contact region crucial for the dimer interface stability.

We thank Dr. Stefano Piana and Dr. Giovanni Settanni for helpful discussions.

REFERENCES

Amadei, A., A. B. Linssen, and H. J. Berendsen. 1993. Essential dynamics of proteins. *Proteins*. 17:412–425.

Berendsen, H. J. C., J. P. M. Postma, W. F. van Gunsteren, A. Di Nola, and J. R. Haak. 1984. *J. Chem. Phys*. 81:3684–3690.

Blanchard, H., L. Kodandapani, P. R. Mittl, S. D. Marco, J. F. Krebs, J. C. Wu, K. J. Tomaselli, and M. G. Grutter. 1999. The three-dimensional structure of caspase-8: an initiator enzyme in apoptosis. *Struct. Fold. Des*. 7:1125–1133.

Brinen, L. S., E. Hansell, J. Cheng, W. R. Roush, J. H. McKerrow, and R. J. Fletterick. 2000. A target within the target: probing cruzain's P1' site to define structural determinants for the Chagas' disease protease. *Struct. Fold. Des*. 8:831–840.

Chillemi, G., M. Falconi, A. Amadei, G. Zimatore, A. Desideri, and A. Di Nola. 1997. The essential dynamics of Cu, Zn superoxide dismutase: suggestion of intersubunit communication. *Biophys. J*. 73:1007–1018.

Cohen, G. M. 1997. Caspases: the executioners of apoptosis. *Biochem. J*. 326:1–16.

Colussi, P. A., N. L. Harvey, L. M. Shearwin-Whyatt, and S. Kumar. 1998. Conversion of procaspase-3 to an autoactivating caspase by fusion to the caspase-2 prodomain. *J. Biol. Chem*. 273:26566–26570.

Coulombe, R., P. Grochulski, J. Sivaraman, R. Menard, J. S. Mort, and M. Cygler. 1996. Structure of human procathepsin L reveals the molecular basis of inhibition by the prosegment. *EMBO J*. 15:5492–5503.

de Groot, B. L., D. M. van Aalten, A. Amadei, and H. J. Berendsen. 1996. The consistency of large concerted motions in proteins in molecular dynamics simulations. *Biophys. J*. 71:1707–1713.

Drenth, J., J. N. Jansonius, R. Koekoek, H. M. Swen, and B. G. Wolthers. 1968. Structure of papain. *Nature*. 218:929–932.

Enari, M., H. Sakahira, H. Yokoyama, K. Okawa, A. Iwamatsu, and S. Nagata. 1998. A caspase-activated DNase that degrades DNA during apoptosis, and its inhibitor ICAD. *Nature*. 391:43–50.

Fengler, A., and W. Brandt. 1998. Three-dimensional structures of the cysteine proteases cathepsins K and S deduced by knowledge-based modelling and active site characteristics. *Protein Eng*. 11:1007–1013.

Fersht, A. 1997. Enzyme Structure and Mechanism. W. H. Freeman and Co., New York.

Garcia, A. E., and G. Hummer. 1999. Conformational dynamics of cytochrome c: correlation to hydrogen exchange. *Proteins*. 36:175–191.

Gillmor, S. A., C. S. Craik, and R. J. Fletterick. 1997. Structural determinants of specificity in the cysteine protease cruzain. *Protein Sci*. 6:1603–1611.

Gilson, M. K., and B. Honig. 1988. Calculation of the total electrostatic energy of a macromolecular system: solvation energies, binding energies, and conformational analysis. *Proteins*. 4:7–18.

Guncar, G., M. Podobnik, J. Pungercar, B. Strukelj, V. Turk, and D. Turk. 1998. Crystal structure of porcine cathepsin H determined at 2.1 Å resolution: location of the mini-chain C-terminal carboxyl group defines cathepsin H aminopeptidase function. *Structure*. 6:51–61.

Guncar, G., G. Pungercic, I. Klemencic, V. Turk, and D. Turk. 1999. Crystal structure of MHC class II-associated p41 Ii fragment bound to cathepsin L reveals the structural basis for differentiation between cathepsins L and S. *EMBO J*. 18:793–803.

Huang, Y., Y. C. Park, R. L. Rich, D. Segal, D. G. Myszka, and H. Wu. 2001. Structural basis of caspase inhibition by XIAP: differential roles of the linker versus the BIR domain. *Cell*. 104:781–790.

Hunenberger, P. 2000. Optimal charge-shaping functions for the particle-particle-particle-mesh (P3M) method for computing electrostatic interactions in molecular simulations. *J. Chem. Phys*. 113:10464–10476.

Jia, Z., S. Hasnain, T. Hirama, X. Lee, J. S. Mort, R. To, and C. P. Huber. 1995. Crystal structures of recombinant rat cathepsin B and a cathepsin B- inhibitor complex. Implications for structure-based inhibitor design. *J. Biol. Chem*. 270:5527–5533.

Johnston, S. C., C. N. Larsen, W. J. Cook, K. D. Wilkinson, and C. P. Hill. 1997. Crystal structure of a deubiquitinating enzyme (human UCH-L3) at 1.8 Å resolution. *EMBO J*. 16:3787–3796.

Johnston, S. C., S. M. Riddle, R. E. Cohen, and C. P. Hill. 1999. Structural basis for the specificity of ubiquitin C-terminal hydrolases. *EMBO J*. 18:3877–3887.

Jordan, J., M. F. Galindo, V. Cena, and C. Gonzalez-Garcia. 2000. Cysteine proteinase and neurodegeneration. *Rev. Neurol*. 31:333–340.

Kamphuis, I. G., K. H. Kalk, M. B. Swarte, and J. Drenth. 1984. Structure of papain refined at 1.65 Å resolution. *J. Mol. Biol*. 179:233–256.

Kaufmann, S. H., and G. J. Gores. 2000. Apoptosis in cancer: cause and cure. *Bioessays*. 22:1007–1017.

Lazebnik, Y. A., S. H. Kaufmann, S. Desnoyers, G. G. Poirier, and W. C. Earnshaw. 1994. Cleavage of poly(ADP-ribose) polymerase by a proteinase with properties like ICE. *Nature*. 371:346–347.

Leach, A. 1996. Molecular Modelling, Principles and Applications. Longman, Harlow, UK.

Lee, D., S. A. Long, J. L. Adams, G. Chan, K. S. Vaidya, T. A. Francis, K. Kikly, J. D. Winkler, C. M. Sung, C. Debouck, S. Richardson, M. A. Levy, W. E. DeWolf, Jr., P. M. Keller, T. Tomaszek, M. S. Head, M. D. Ryan, R. C. Haltiwanger, P. H. Liang, C. A. Janson, P. J. McDevitt, K. Johanson, N. O. Concha, W. Chan, S. S. Abdel-Meguid, A. M. Badger, M. W. Lark, D. P. Nadeau, L. J. Suva, M. Gowen, and M. E. Nuttall. 2000. Potent and selective nonpeptide inhibitors of caspases 3 and 7 inhibit apoptosis and maintain cell functionality. *J. Biol. Chem*. 275: 16007–16014.

Lindahl, E., B. Hess, and D. van der Spoel. 2001. Gromacs 3.0: a package for molecular simulation and trajectory analysis. *J. Mol. Mod*. 7:306–317.

Liu, X., H. Zou, C. Slaughter, and X. Wang. 1997. DFF, a heterodimeric protein that functions downstream of caspase-3 to trigger DNA fragmentation during apoptosis. *Cell*. 89:175–184.

Mittl, P. R., S. Di Marco, J. F. Krebs, X. Bai, D. S. Karanewsky, J. P. Priestle, K. J. Tomaselli, and M. G. Grütter. 1997. Structure of recombinant human CPP32 in complex with the tetrapeptide acetyl-Asp-Val-Ala-Asp fluoromethyl ketone. *J. Biol. Chem*. 272:6539–6547.

Musil, D., D. Zucic, D. Turk, R. A. Engh, I. Mayr, R. Huber, T. Popovic, V. Turk, T. Towatari, N. Katunuma, et al.1991. The refined 2.15 Å X-ray crystal structure of human liver cathepsin B: the structural basis for its specificity. *EMBO J*. 10:2321–2330.

Muzio, M., B. R. Stockwell, H. R. Stennicke, G. S. Salvesen, and V. M. Dixit. 1998. An induced proximity model for caspase-8 activation. *J. Biol. Chem*. 273:2926–2930.

Nicholson, D. W., A. Ali, N. A. Thornberry, J. P. Vaillancourt, C. K. Ding, M. Gallant, Y. Gareau, P. R. Griffin, M. Labelle, Y. A. Lazebnik, et al. 1995. Identification and inhibition of the ICE/CED-3 protease necessary for mammalian apoptosis. *Nature*. 376:37–43.

Okamoto, Y., H. Anan, E. Nakai, K. Morihira, Y. Yonetoku, H. Kurihara, H. Sakashita, Y. Terai, M. Takeuchi, T. Shibanuma, and Y. Isomura. 1999. Peptide based interleukin-1 beta converting enzyme (ICE) inhibitors: synthesis, structure activity relationships and crystallographic study of the ICE-inhibitor complex. *Chem. Pharm. Bull. (Tokyo)*. 47:11–21.

Piana, S., P. Carloni, and M. Parrinello. 2002. Role of conformational fluctuations in the enzymatic reaction of HIV-1 protease. *J. Mol. Biol.* 319:567–83.

Porter, A. G., and R. U. Janicke. 1999. Emerging roles of caspase-3 in apoptosis. *Cell Death Differ.* 6:99–104.

Radkiewicz, J., and C. Brooks. 2000. Protein dynamics in enzymatic catalysis: exploration of dihydrofolate reductase. *J. Am. Chem. Soc.* 122:225–231.

Rano, T. A., T. Timkey, E. P. Peterson, J. Rotonda, D. W. Nicholson, J. W. Becker, K. T. Chapman, and N. A. Thornberry. 1997. A combinatorial approach for determining protease specificities: application to interleukin-1beta converting enzyme (ICE). *Chem. Biol.* 4:149–155.

Renatus, M., H. R. Stennicke, F. L. Scott, R. C. Liddington, and G. S. Salvesen. 2001. Dimer formation drives the activation of the cell death protease caspase 9. *Proc. Natl. Acad. Sci. USA.* 98:14250–14255.

Riedl, S. J., M. Renatus, R. Schwarzenbacher, Q. Zhou, C. Sun, S. W. Fesik, R. C. Liddington, and G. S. Salvesen. 2001. Structural basis for the inhibition of caspase-3 by XIAP. *Cell.* 104:791–800.

Rotonda, J., D. W. Nicholson, K. M. Fazil, M. Gallant, Y. Gareau, M. Labelle, E. P. Peterson, D. M. Rasper, R. Ruel, J. P. Vaillancourt, N. A. Thornberry, and J. W. Becker. 1996. The three-dimensional structure of apopain/CPP32, a key mediator of apoptosis. *Nat. Struct. Biol.* 3: 619–625.

Ryckaert, J. P., G. Ciccotti, and H. J. C. Berendsen. 1977. Numerical integration of the cartesian equations of motion of a system with constraints: molecular dynamics of n-alkanes. *J. Comp. Phys.* 23: 327–341.

Salvesen, G. S., and V. M. Dixit. 1997. Caspases: intracellular signaling by proteolysis. *Cell.* 91:443–446.

Shimohama, S. 2000. Apoptosis in Alzheimer's disease–an update. *Apoptosis.* 5:9–16.

Stennicke, H. R., and G. S. Salvesen. 1997. Biochemical characteristics of caspases-3, -6, -7, and -8. *J. Biol. Chem.* 272:25719–25723.

Sulpizi, M., A. Laio, J. VandeVondele, U. Rothlisberger, and P. Carloni. 2003. *Proteins.* In press.

Sussman, J. L., D. Lin, J. Jiang, N. O. Manning, J. Prilusky, O. Ritter, and E. E. Abola. 1998. Protein Data Bank (PDB): database of three-dimensional structural information of biological macromolecules. *Acta Crystallogr. D Biol. Crystallogr.* 54:1078–1084.

Talanian, R. V., K. D. Brady, and V. L. Cryns. 2000. Caspases as targets for anti-inflammatory and anti-apoptotic drug discovery. *J. Med. Chem.* 43:3351–3371.

Talanian, R. V., L. C. Dang, C. R. Ferenz, M. C. Hackett, J. A. Mankovich, J. P. Welch, W. W. Wong, and K. D. Brady. 1996. Stability and oligomeric equilibria of refolded interleukin-1beta converting enzyme. *J. Biol. Chem.* 271:21853–21858.

Thompson, S. K., S. M. Halbert, M. J. Bossard, T. A. Tomaszek, M. A. Levy, B. Zhao, W. W. Smith, S. S. Abdel-Meguid, C. A. Janson, K. J. D'Alessio, M. S. McQueney, B. Y. Amegadzie, C. R. Hanning, R. L. DesJarlais, J. Briand, S. K. Sarkar, M. J. Huddleston, C. F. Ijames, S. A. Carr, K. T. Garnes, A. Shu, J. R. Heys, J. Bradbeer, D. Zembryki, D. F. Veber, et al.1997. Design of potent and selective human cathepsin K inhibitors that span the active site. *Proc. Natl. Acad. Sci. USA.* 94:14249–14254.

Turk, D., M. Podobnik, T. Popovic, N. Katunuma, W. Bode, R. Huber, and V. Turk. 1995. Crystal structure of cathepsin B inhibited with CA030 at 2.0-A resolution: a basis for the design of specific epoxysuccinyl inhibitors. *Biochemistry.* 34:4791–4797.

van Gunsteren, W. F., S. R. Billeter, A. A. Eising, P. H. Hünenberger, P. K. H. C. Krüger, A. E. Mark, W. R. P. Scott, and I. G. Tironi. 1996. Biomolecular Simulation: The GROMOS96 Manual and User Guide. vdf Hochschulverlag AG, Zürich.

Ventimiglia, R., L. Lau, R. Kinloch, A. Hopkins, E. Karran, L. Petalidis, and R. Ward. 2001. Role of caspases in neuronal apoptosis. *Drug Dev. Res.* 52:525–533.

Walker, N. P., R. V. Talanian, K. D. Brady, L. C. Dang, N. J. Bump, C. R. Ferenz, S. Franklin, T. Ghayur, M. C. Hackett, L. D. Hammill, et al.1994. Crystal structure of the cysteine protease interleukin-1 beta-converting enzyme: a (p20/p10)2 homodimer. *Cell.* 78:343–352.

Watt, W., K. A. Koeplinger, A. M. Mildner, R. L. Heinrikson, A. G. Tomasselli, and K. D. Watenpaugh. 1999. The atomic-resolution structure of human caspase-8, a key activator of apoptosis. *Struct. Fold. Des.* 7:1135–1143.

Wei, Y., T. Fox, S. P. Chambers, J. Sintchak, J. T. Coll, J. M. Golec, L. Swenson, K. P. Wilson, and P. S. Charifson. 2000. The structures of caspases-1, -3, -7 and -8 reveal the basis for substrate and inhibitor selectivity. *Chem. Biol.* 7:423–432.

Wilson, K. P., J. A. Black, J. A. Thomson, E. E. Kim, J. P. Griffith, M. A. Navia, M. A. Murcko, S. P. Chambers, R. A. Aldape, S. A. Raybuck, et al.1994. Structure and mechanism of interleukin-1 beta converting enzyme. *Nature.* 370:270–275.

Xu, G., M. Cirilli, Y. Huang, R. L. Rich, D. G. Myszka, and H. Wu. 2001. Covalent inhibition revealed by the crystal structure of the caspase- 8/p35 complex. *Nature.* 410:494–497.

Yamamoto, A., K. Tomoo, T. Hara, M. Murata, K. Kitamura, and T. Ishida. 2000. Substrate specificity of bovine cathepsin B and its inhibition by CA074, based on crystal structure refinement of the complex. *J. Biochem. (Tokyo).* 127:635–643.

Yamashita, D. S., W. W. Smith, B. G. Zhao, C. A. Janson, T. A. Tomaszek, M. J. Bossard, M. A. Levy, H. J. Oh, T. J. Carr, S. K. Thompson, C. F. Ijames, S. A. Carr, M. McQueney, K. J. D'Alessio, B. Y. Amegadzie, C. R. Hanning, S. Abdelmeguid, R. L. DesJarlais, J. G. Gleason, and D. F. Veber. 1997. Structure and design of potent and selective cathepsin K inhibitors. *J. Am. Chem. Soc.* 119:11351–11352.

Yang, X., H. Y. Chang, and D. Baltimore. 1998. Autoproteolytic activation of pro-caspases by oligomerization. *Mol. Cell.* 1:319–325.

Zhao, B., C. A. Janson, B. Y. Amegadzie, K. D'Alessio, C. Griffin, C. R. Hanning, C. Jones, J. Kurdyla, M. McQueney, X. Qiu, W. W. Smith, and S. S. Abdel-Meguid. 1997. Crystal structure of human osteoclast cathepsin K complex with E-64. *Nat. Struct. Biol.* 4:109–111.